XMM-Newton CCF Release Note

XMM-CCF-REL-272

EPIC MOS response

S. Sembay, R. D. Saxton, M. Guainazzi

31 Jan 2011

1 CCF components

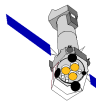| Name of CCF	VALDATE	EVALDATE	Blocks changed	XSCS flag
EMOSn_REDIST_0080.CCF	1999-12-10	2000-10-03	CCD_REDISTRIBUTION-n	NO
EMOSn_REDIST_0081.CCF	2000-10-03	2001-04-22	CCD_REDISTRIBUTION-n	NO
EMOSn_REDIST_0082.CCF	2001-04-22	2001-11-07	CCD_REDISTRIBUTION-n	NO
EMOSn_REDIST_0083.CCF	2001-11-07	2002-05-26	CCD_REDISTRIBUTION-n	NO
EMOSn_REDIST_0084.CCF	2002-05-26	2002-11-05	CCD_REDISTRIBUTION-n	NO
EMOSn_REDIST_0085.CCF	2002-11-05	2004-01-14	CCD_REDISTRIBUTION-n	NO
EMOSn_REDIST_0086.CCF	2004-01-14	2005-02-14	CCD_REDISTRIBUTION-n	NO
EMOSn_REDIST_0087.CCF	2005-02-14	2006-03-22	CCD_REDISTRIBUTION-n	NO
EMOSn_REDIST_0088.CCF	2006-03-22	2007-04-24	CCD_REDISTRIBUTION-n	NO
EMOSn_REDIST_0089.CCF	2007-04-24	2008-05-28	CCD_REDISTRIBUTION-n	NO
EMOSn_REDIST_0090.CCF	2008-05-28	2009-07-01	CCD_REDISTRIBUTION-n	NO
EMOSn_REDIST_0091.CCF	2009-07-01	2010-08-03	CCD_REDISTRIBUTION-n	NO
EMOSn_REDIST_0092.CCF	2010-08-03	NONE	CCD_REDISTRIBUTION-n	NO

Where the n refers to the MOS-1 and MOS-2 cameras in *EMOSn* and to the 7 CCDs of each camera in *CCD_REDISTRIBUTION-n*.

2 Changes

This release introduces a major change in the modeling of the redistribution function for the MOS detectors. The detector response had previously been calculated using a physical model but it has been seen that an empirical parameterisation can actually better reproduce the spatially-dependent, time-dependent redistribution (RMF).

The modified CCFs are compatible with SAS versions 11 and later, which implements the new algorithm. Earlier versions of the SAS, working with these CCFs, will exit with an error message.

The new model of the MOS RMF is a phenomenological description of the shape of the redistribution function as a function of energy for the various regions and epochs as de-

fined. Figure 1 shows ground calibration data of the response to 425 eV input photons for MOS1 CCD1. The response has a characteristic secondary peak whose relative strength is known to vary as a function of energy. The in-flight calibration data is consistent with it being this component which is evolving spatially and with time.

Figure 2 shows an example model RMF for three regions, the patch core, the patch wings and the outer CCD region also for an input energy of 425 eV. We have modelled the shape of the RMF with functions which give a good representation of the ground data but which can be modified via the scheme described below to find the best fit to in-flight data. Essentially the evolution observed is consistent with the secondary peak appearing at lower relative energies and the overall shape of the response below the main photopeak being flatter.

The response is now specified at 13 different epochs, summarised in table 1. Spatial regions remain as before with an on-patch region (radius 14 CCD pixels), a wings-of-patch region (annulus of 14–36 CCD pixels) and an off-patch region.

An iterative minimsation scheme has been developed to derive the redistribution parameters for a given epoch and chip region by finding the best *simultaneous* fit to MOS data using spectral models of astrophysical sources and the onboard calibration source (used to constrain the RMF at 5.8–6.5 keV, the energy of the Mn Kα calibration lines).

The astrophysical sources constitute two groups. The first group are the line dominated sources 1ES0102-72.3 (a SNR) and Zeta Puppis (an O star). The spectral models for these objects have been derived primarily from RGS data (e.g. Plucinksy et al. 2008). They provide constraints on the redistribution function in the band 0.3-2.5 keV. The sources are very stable and we assume the same input spectral model for all epochs (although the fitting procedure allows some variation in the relative normalisation between the spectral model and the MOS data).

The second group comprise soft point sources such as the isolated neutron stars RX J1856.3154 and RX J0720.4-3125, the white dwarf CAL 83 and the soft excess AGN MRK 279. In these cases we have used spectral models derived from simultaneous EPIC-pn data. This group has been used to constrain the redistribution function in the energy range 0.2 to 1.0 keV (and therefore overlaps the first group).

The methodology for deriving the MOS RMF is therefore dependant on both the current calibration of the EPIC-pn and the RGS and is not independent of these instruments. The calibration of all instruments has been modified since launch with reference to information supplied by the other instruments and this new calibration scheme of the MOS can be viewed in this light.

The observations used in the fits are given in table 2. Currently, parameters for epochs 1,2,4,6,7,9 and 12 have been calculated using the procedure above and the other epochs have been interpolated. Epoch 13 is a direct copy of epoch 12 in this release.

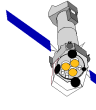An example of the effect on the RMF introduced by this release is shown in figure 3.

Table 1: Epochs of MOS response

Epoch	Revolutions	Dates[a]
1	0-150	1999-12-10 to 2000-10-02
2	151–250	2000-10-03 to 2001-04-21
3	251–350	2001-04-22 to 2001-11-06
4	351–450	2001-11-07 to 2002-05-25
5	451–532	2002-05-26 to 2002-11-04
6	533–750	2002-11-05 to 2004-01-13
7	751–950	2004-01-14 to 2005-02-13
8	951–1150	2005-02-14 to 2006-03-21
9	1151–1350	2006-03-22 to 2007-04-23
10	1351–1550	2007-04-24 to 2008-05-27
11	1551–1750	2008-05-28 to 2009-06-30
12	1751–1950	2009-07-01 to 2010-08-02
13	1951–	2010-08-03 to

[a] From the beginning of the first date to the end of the second.

Table 2: Observations used in the derivation of the RMF

| Revolution	Epoch	Obsid	Source
65	1	0123110201	1ES0102-72.3
65	1	0123110301	1ES0102-72.3
68	1	0123510101	Cal 83
156	2	0095810401	Zeta Puppis
175	2	0132520301	RX J0720.4-3125
247	2	0135720601	1ES0102-72.3
375	4	0135720801	1ES0102-72.3
427	4	0106260101	RX J1856.5-3754
441	4	0083960101	MRK 279
447	4	0135721001	1ES0102-72.3
636	6	0159360101	Zeta Puppis
711	6	0161960201	RX J0720.4-3125
711	6	0135721501	1ES0102-72.3
795	7	0159360301	Zeta Puppis
878	7	0165971601	RX J1856.5-3754
878	7	0165971701	RX J1856.5-3754
888	7	0135722401	1ES0102-72.3
894	7	0135722001	1ES0102-72.3
900	7	0135722101	1ES0102-72.3
900	7	0135722201	1ES0102-72.3
900	7	0135722301	1ES0102-72.3
903	7	0159360401	Zeta Puppis
1165	9	0135722701	1ES0102-72.3
1259	9	0412600101	RX J1856.5-3754
1265	9	0412980101	1ES0102-72.3
1335	9	0415180101	RX J1856.5-3754
1343	9	0414400101	Zeta Puppis
1814	12	0561380101	Zeta Puppis
1883	12	0412600901	RX J1856.5-3754
1898	12	0412981001	1ES0102-72.3
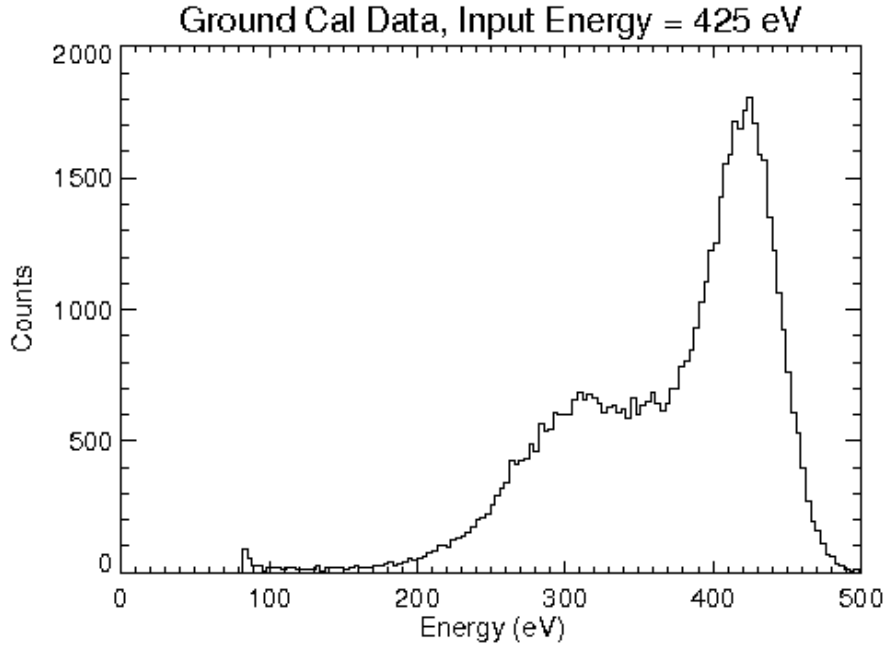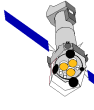
Figure 1: A plot of the redistribution function at 425 eV, measured in ground calibration observations.

3   Scientific Impact of this Update

An assessment of the impact of this change has been made by performing fits of MOS and EPIC-pn data on observations of calibration sources made throughout the mission. The best-fit χ^2 and the relative camera in-band fluxes have been investigated. Examples of fits with the old and new MOS response files are shown in Fig. 4 for a very soft continuum source, located on the core of the patch, and a line-dominated source, located in the wings. It can be clearly seen that the new RMF is a better description of the data below ∼0.6 keV.

Within the patch region the RMF evolves strongly with time. To check the performance of the new RMFs at all epochs, a comparison of the change in χ^2 for the two MOS cameras has been made for observations spanning the duration of the mission (Fig. 5). A general improvement is seen which becomes particularly strong after revolution ∼1000 (especially for MOS-1). In the very latest observations (epoch 13) the trend may be reversed and this epoch still requires attention. A similar comparison with many sources from the XCAL archive (Stuhlinger et al. 2010), yields a general reduction in χ^2 with the new matrices which becomes important for several observations which were poorly fit previously (Fig. 6).

Although there are many factors which influence the relative fluxes recorded by the EPIC cameras, it is interesting to see what effect this change makes. In Fig. 7 we plot a histogram of the ratios of the MOS to EPIC-pn fluxes for 6 energy bands, for sources from the XCAL archive. The ratio becomes closer to the desired 1.0 in the MOS-1, 0.33-
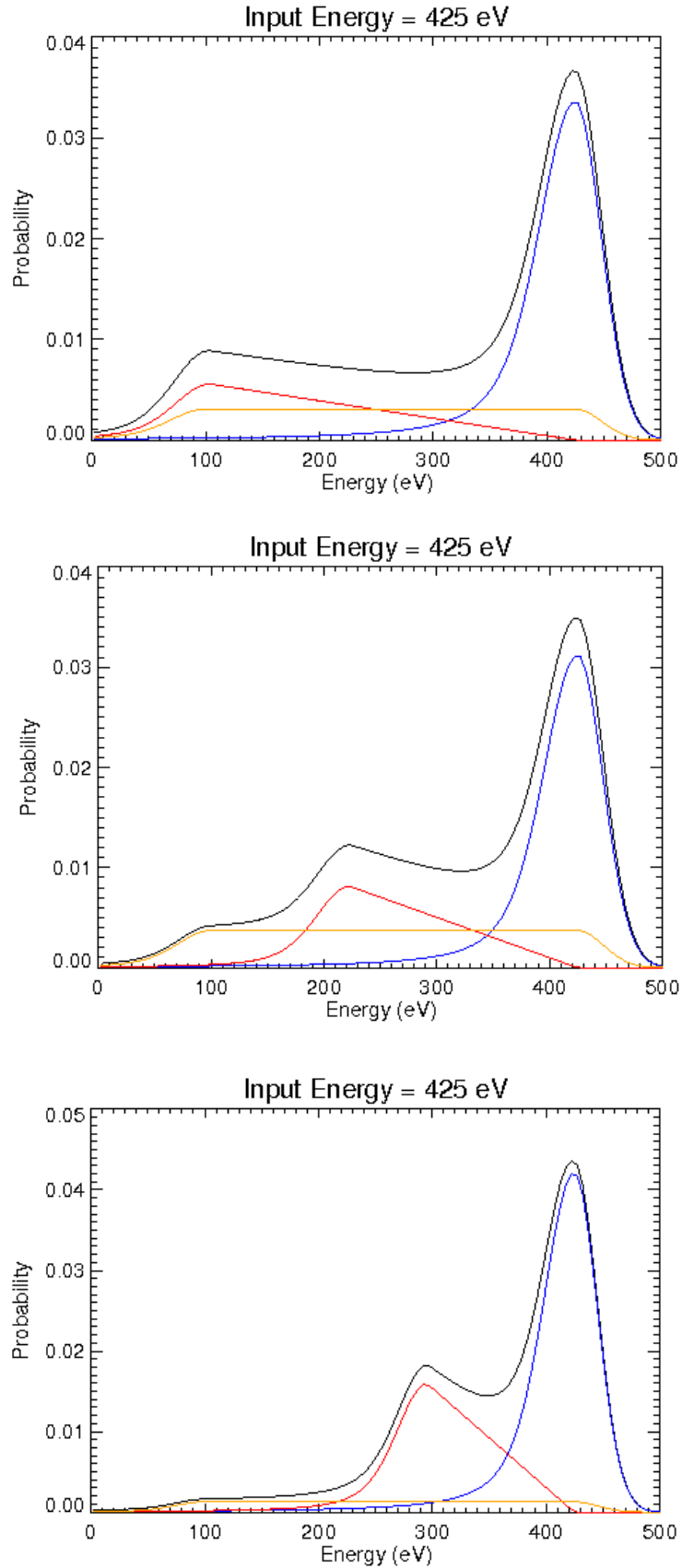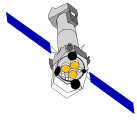
Figure 2: The model RMF at 425 eV for three regions; on the patch (upper), in the wings of the patch (middle) and off patch (lower).
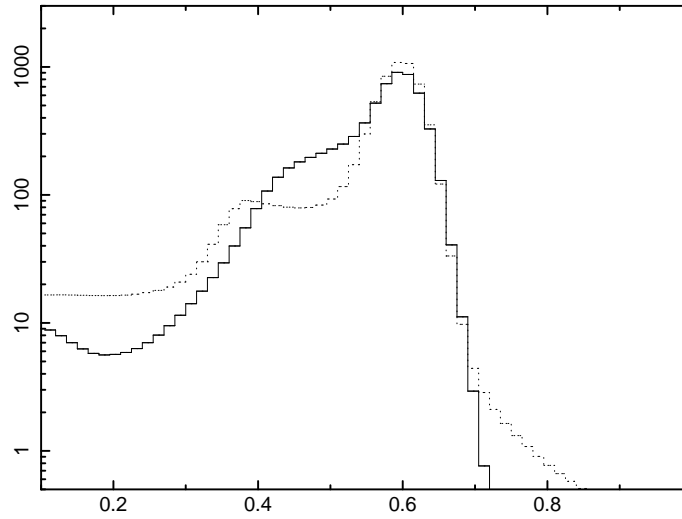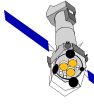
Figure 3: A plot of the old (solid line) and new (dashed line) RMFs at 0.6 keV for an on-patch source observed in rev 451 (epoch 4).

0.54 and 0.54-0.85 keV bands and in the MOS-2, 0.33-0.54 keV band. The impact on the other bands is less obvious.

4   Estimated Scientific Quality

This release gives a noticeable improvement in spectral fits at energies from 0.3–0.85 keV, particularly for observations made since revolution 1000 (May 2005). There remain residual errors in epoch 13 indicating that further adjustments will be needed.

The impact on the best-fit parameters is significant on a sample of blazars taken from the XCAL archive, yielding larger-than-statistical-error changes in both the column density and the soft component spectral index in a broken power-law model fit (Fig. 8). The effect of the new RMFs is to steepen the measured power-law slope by ~ 0.2 and increase the measured N_H for both MOS-1 and MOS-2, for sources observed after revolution 532.

5   Test procedures and results

Reponse matrices have been generated for sources observed near to the optical-axis, for a range of dates, for both of the MOS cameras. This successfully tests the creation of RMFs with the new algorithm, for sources, whose photons fall predominantly on the patch and in the wings of the patch.
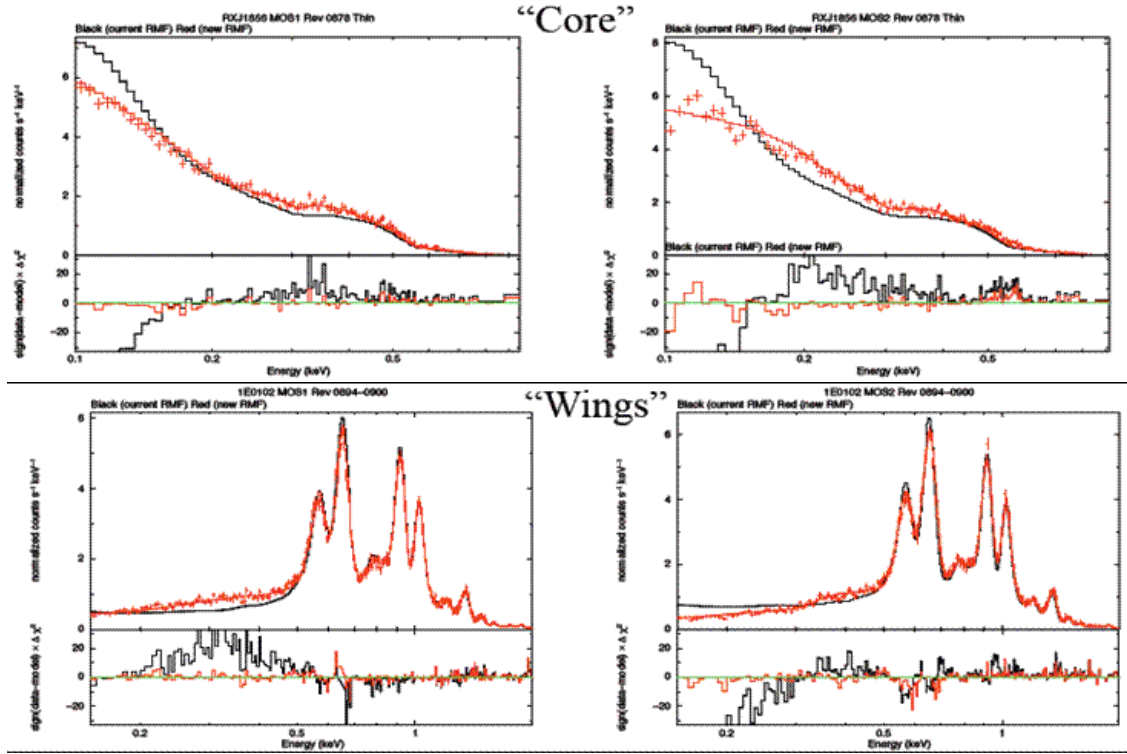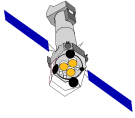
Figure 4: A comparison of spectral fits to RXJ 1856.6-37541 (upper) and 1E0102.2-7219 (lower), using the current (black line) and new (red line) RMFs for MOS-1 (left) and MOS-2 (right).
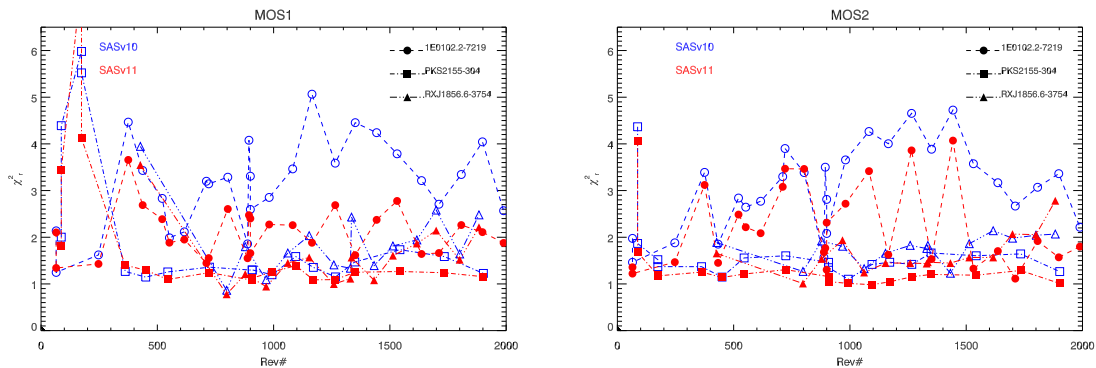

Figure 5: A comparison of χ^2_r from spectral fits to 1E102.2-7219, PKS 2155-304 and RXJ 1856.6-3754, using the current (open symbols) and new (closed symbols) RMFs as a function of revolution number. Left panel: MOS-1; Right panel: MOS-2.
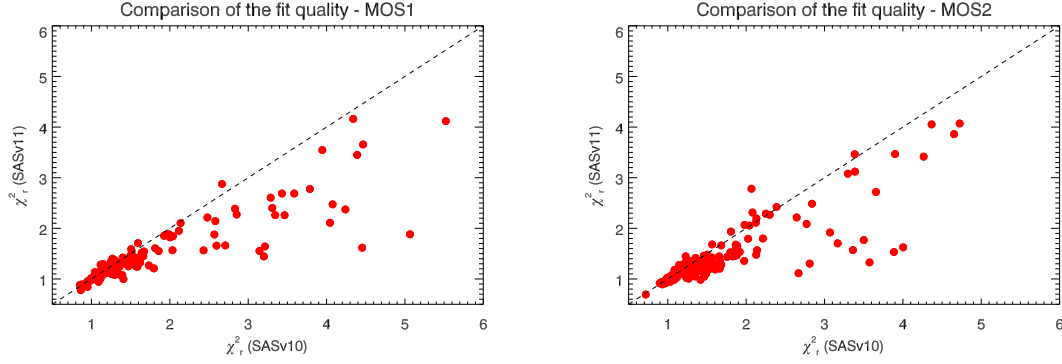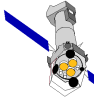
Figure 6: A comparison of χ_r^2 from fits to MOS-1 (left) and MOS-2 (right) spectra of a sample of sources from the XCAL archive using the old (SASv10; X-axis) and new (SASv11 + the new CCFs; Y-axis) RMF algorithms.

6   References

Plucinksy et al. 2008, SPIE, 7011, 68
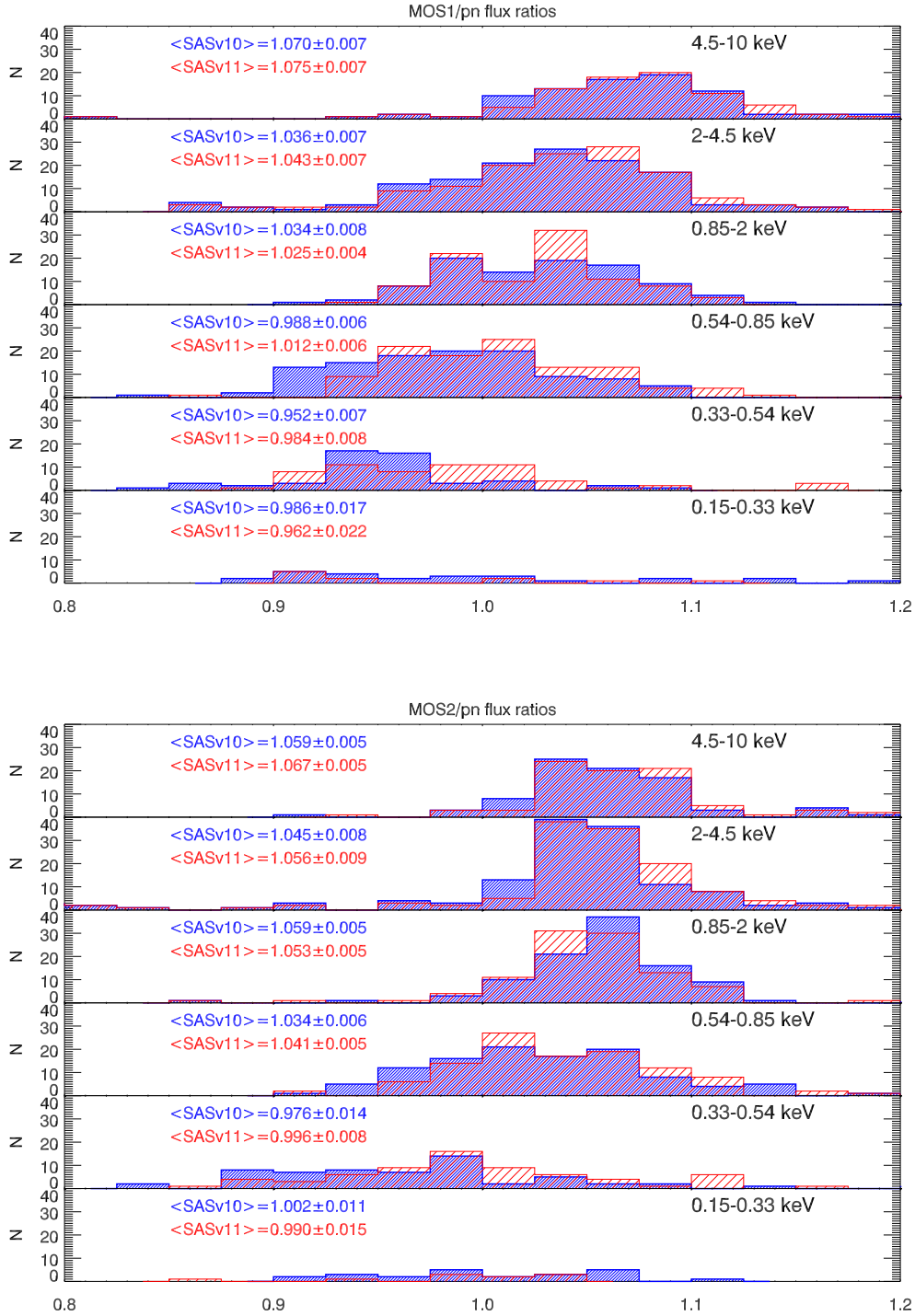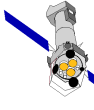Stuhlinger et al. 2010, XMM-SOC-CAL-TN-0052

Figure 7: The ratio of MOS-1 to PN flux (upper panel) and MOS-2 to PN flux (lower panel) after joint fits to a sample of sources from the XCAL archive. The hashed red histograms indicate the ratios using the new RMFs and the hashed blue blocks use the old RMFs. Subpanels from bottom to top indicate the 0.15–0.33, 0.33–0.54, 0.54–0.85, 0.85–2.0, 2.0–4.5 and 4.5–10 keV bands.
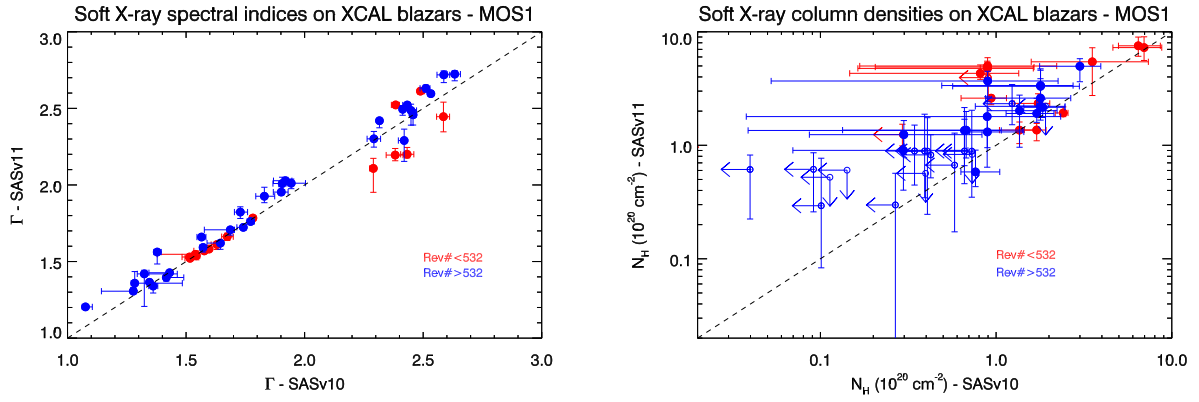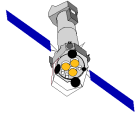
Figure 8: Soft X-ray spectral slopes (left) and absorption columns (right) returned by fits of an absorbed broken power-law to a set of blazar spectra for the old (SASv10) and new (SASv11 + these CCFs) RMFs. Open symbols represent sources with upper limits in at least one of the measured quantities.